

# The thermodynamics of hydride precipitation: the importance of entropy, enthalpy and disorder

S. C. Lumley<sup>a,d</sup>, R. W. Grimes<sup>a</sup>, S. T. Murphy<sup>a</sup>, P. A. Burr<sup>a,b</sup>, A. Chroneos<sup>a,c</sup>, P. R. Chard-Tuckey<sup>d</sup>, M. R. Wenman<sup>a,\*</sup>

<sup>a</sup>Centre for Nuclear Engineering and Department of Materials, Imperial College London, London, SW7 2AZ, UK.

<sup>b</sup>Institute of Materials Engineering, Australian Nuclear Science & Technology Organisation, Menai, New South Wales 2234, Australia.

<sup>c</sup>Engineering and Innovation, The Open University, Milton Keynes MK7 6AA, UK.

<sup>d</sup>Nuclear Department, Defence Academy, HMS Sultan, Gosport, Hampshire, PO12 3BY, UK.

---

## Abstract

The precipitation of zirconium hydrides from Zr solid solution was investigated using first principles lattice dynamics simulations. These included the temperature dependent vibrational enthalpy and vibrational entropy combined with the configurational entropy terms. In contrast with previous approaches, it was found that the latent enthalpy alone is not sufficient to fully describe precipitation of hydrides; a full thermodynamical assessment is required. In particular the vibrational enthalpy of precipitation assists in stabilising HCP hydrides and is especially important in forming the metastable  $\zeta$  phase. The configurational entropy change during precipitation favours FCC hydrides. Given this, at concentrations below 300 ppm H, no hydride precipitation is predicted, suggesting that when hydrides are seen in those materials it is because the local concentration of H is greater than that measured globally. While  $\gamma$  hydride is the most stable phase, it is very close in energy to the  $\delta$  phase.

---

## 1. Introduction

Zr alloys are used for fuel cladding and other in-core structures in water cooled nuclear reactors due to their good mechanical and corrosion properties and low capture cross-section for thermal neutrons. The uptake of H and its precipitation as hydrides in Zr alloys is important in the ongoing development of fuel cladding for water cooled reactors [1]. At reactor operating temperatures, H is soluble up to around 100 ppm and extremely mobile in  $\alpha$ -Zr [2, 3, 5]. However, if sufficient H is present or if the solubility limit of H in  $\alpha$ -Zr is lowered (commonly due to a reduction in temperature during reactor transients [6]), then H will precipitate out, forming zirconium hydrides. The hydrides are brittle and cause component degradation and may lead to failure of the fuel cladding; this is especially likely if they align along the radial direction

---

\*Corresponding author. E-mail address: m.wenman@imperial.ac.uk, Telephone: +44(0)20 7594 6763, Fax: +44(0)20 7594 6729.

10 of the fuel pin due to stress reorientation [1, 4]. Recently proposed changes in the regulations for nuclear  
11 fuel cladding to limit H uptake [7] and proposals for ever longer dry storage times [8] make understanding  
12 H solubility and hydride precipitation increasingly important for operators and manufacturers alike.

13 Current understanding suggests that there are five main ways that H can be sequestered in Zr metal;  
14 these are, the formation of four hydrides ( $\zeta$ ,  $\gamma$ ,  $\delta$  and  $\varepsilon$ ) and the solid solution in Zr [9, 10, 11, 12]. The  
15 structures of these different hydrides are shown in Fig. 1. There is a general relationship of decreasing  
16  $c/a$  ratio with increasing H content. Of particular interest is that the most commonly observed  $\delta$  phase is  
17 often reported to have a formula of  $\text{ZrH}_{1.66}$  and a disordered fluorite structure, while simulators often use  
18 a simplified ersatz of periodic  $\text{ZrH}_{1.5}$  [12, 13]. The  $\gamma$  hydride has been assumed to be metastable, as it is  
19 less readily observed than the  $\delta$  hydride [14]. However, other investigations have observed the  $\gamma$  hydride  
20 at room temperature [15], under both slow cooling [10] and fast cooling regimes [16]. Overall, it appears  
21 that the stability and occurrence of these phases is a complex phenomenon, where the H concentration,  
22 thermal treatments, alloying additions and stress states all have a part to play in determining which phases  
23 are observed [17].

24 The focus of this study is on modelling hydrides using *ab initio* atomistic simulation techniques based on  
25 density functional theory (DFT). In  $\alpha$ -Zr metal, H preferentially occupies tetrahedral sites in the Zr lattice,  
26 rather than other sites [12, 18, 19]. Some works have focused on the octahedral site as the main location  
27 for H atom solution, however such works appear to be in the minority [20, 21]. It has been theoretically  
28 predicted that the FCT structure of  $\text{ZrH}_2$  can have another stable phase for  $c/a$  greater than 1 [22, 23]. Zhu  
29 *et al.* [13] studied the ordered hydride phases using DFT; they concluded that  $\delta \text{ZrH}_{1.5}$  is thermodynamically  
30 less stable than the other phases at high temperature. Zhong and MacDonald, who published previous DFT  
31 results combined with new calculations of the  $\gamma$  phase, suggest the  $\gamma$  phase is stable at temperatures below  
32 about 523 K [24].

33 The simulation of hydrides is complicated due to the random distribution of the H atoms in some phases.  
34 Although hydrides have been simulated in the past, few studies have attempted to examine hydrides whilst  
35 taking into account the disorder. One of the most successfully used techniques for simulating disordered  
36 atomic structures is the special quasi-random structures (SQS) method developed by Zunger *et al.* [25], which  
37 has been used to simulate a range of non-stoichiometric materials and structures. It has also recently been  
38 applied to this system [26]. In this study SQS techniques are combined with a statistical analysis of a large  
39 number of randomly generated cells, in order to examine the impact of disorder on hydride precipitation.  
40 Phonon calculations are also used to calculate thermodynamic properties such as the vibrational entropy and  
41 the sensible enthalpy changes during precipitation. Previous studies on other systems by DFT have shown  
42 the importance of vibrational entropy on the solubility limit in precipitation reactions from solid solution,  
43 and its importance in creating a temperature dependent understanding of hydride precipitation [27, 28].  
44 Thus, a comprehensive view of the enthalpy and entropic contributions towards hydride precipitation in Zr

45 is developed.

## 46 **2. Methodology**

### 47 *2.1. Simulation Parameters*

48 For this investigation, CASTEP 5.5 was used to simulate the different structures [29]. As a plane-  
49 wave pseudopotential code, it is particularly appropriate for modelling crystals. Ultrasoft pseudopotentials  
50 were generated “on-the-fly”, under the formalisation of Vanderbilt *et al.* [30]. Valence electrons for Zr were  
51 modelled as  $4s^2 4p^6 5s^2 4d^2$ . Convergence with respect to basis-set cut-off energy and k-point grid density was  
52 tested in a series of electronic self consistency calculations. It was found that the simulations were accurate  
53 to 2 d.p. for a cut-off energy of 400 eV and a k-point grid spaced of  $0.3 \text{ nm}^{-1}$ . k-points were arranged in a  
54 gamma-centred Monkhorst-Pack grid [31]. As the system displays metallic characteristics, the integration  
55 of the Brillouin zone is achieved via a Methfessel-Paxton scheme, with a band smearing width of 1 eV [32].

56 All cells used in this work are geometry relaxed in order to approach their minimum energy configuration.  
57 Cells were considered relaxed when the difference between two successively modified iterations were below  
58 all of the following criteria:

- 59 • Energy derivative  $< 0.001 \text{ eV}$
- 60 • Force on ions  $< 0.5 \text{ eV nm}^{-1}$
- 61 • Displacement of ions derivative  $< 0.01 \text{ nm}^{-1}$
- 62 • Total stress derivative  $< 0.1 \text{ GPa}$

63 Relaxation of atomic positions was carried out under the quasi-Newtonian BFGS scheme [33]. Both  
64 atomic positions within the cell, the lattice constants and cell aspect ratios were unconstrained during  
65 relaxation. This means that volume and cell distortions due to H accommodation are fully accounted for.  
66 Previous works [1, 34, 4] showed that constrained expansion of the hydrides may affect DHC, however, that  
67 is beyond the scope of the current work.

### 68 *2.2. Thermodynamic Considerations*

69 With static simulations it is usual to consider the energy change from a set of reactants to a set of  
70 products. Relating the calculated energy changes to a real system is often difficult, as there are numerous  
71 different energy components, while static calculations can directly only evaluate the ground state changes  
72 (ie. the latent enthalpy of a reaction). Thus, many factors present in a real system are not represented in a  
73 simulation. These different components and factors are often poorly communicated between experimentalists

74 and simulators, leading to inappropriate assumptions when using terms such as energy, enthalpy and entropy.  
75 To ensure a clear understanding, the terms that were calculated here are now discussed.

76 The fundamental measure of the driving force behind a reaction is the Gibbs free energy change:

$$\Delta G = \Delta H - T\Delta S \quad (1)$$

77 where  $\Delta H$  represents the enthalpy change of the system and  $\Delta S$  represents the entropy change. There are  
78 different contributors to the enthalpic and entropic terms, thus Eq. 1 can be expanded into:

$$\Delta G(T) = (\Delta H_l + \Delta H_s(T)) - T(\Delta S_v(T) + \Delta S_{cl}) \quad (2)$$

79 where:

- 80 •  $\Delta H_l$  is the latent enthalpy associated with the reaction. It is due simply to the formation or destruction  
81 of bonds and is independent of external conditions. When quoting results from DFT simulations, this  
82 is the most commonly reported number. If the other terms are ignored this is often quoted as the  
83 energy.
- 84 •  $\Delta H_s$  is the sensible enthalpy and is related to the heat capacities of the different species involved in the  
85 reaction. In order to calculate this, the amount of thermal energy that can be stored in the lattice needs  
86 to be known. This is achieved by calculating the phonon density of states of the materials in question,  
87 and integrating the different acoustic modes in the harmonic approximation, for a temperature  $T$ .
- 88 •  $\Delta S_v$  is the vibrational entropy and is a function of the number of discrete vibrational energy levels  
89 that exist amongst the different acoustic modes of the system. This is determined by the application  
90 of the Boltzmann entropy equation to the harmonic approximation of the phonon distribution [35].
- 91 •  $\Delta S_{cl}$  is the lattice component of the configurational entropy. This only applies to solids with a  
92 disordered lattice, which in this system consists of the H sub-lattice. An approximation of this is  
93 reported in section 3.4.

94 It is clear that the distribution of phonons must be calculated in order to determine two of the terms  
95 included here. Analysis of phonon distributions has been previously examined in this system by Blomqvist  
96 *et al.* [23]. In the present study, this was achieved by means of the finite displacement method, in the (direct)  
97 supercell approach [36].

98 In a real precipitation event, there would be stress related effects, as well as contributions arising from the  
99 creation of a hydride-Zr interface. There would also be entropy created by intrinsic defects on the Zr lattice.  
100 This study cannot comment on such effects, as they would require simulations that are either significantly  
101 larger than the scale that DFT presently allows, or an exceedingly large number of simulations. However,

102 the numbers produced in this work represent a large portion of the overall driving forces for precipitation,  
103 and are a significant advance on what has been achieved for this system previously.

### 104 2.3. Cell Configurations

105 This study examines both ordered and disordered models of hydrides and Zr-H solid solutions. The  
106 ordered models are performed by a straight-forward geometry optimisation of hydride structures including  
107 the commonly accepted structures of  $\zeta$ -Zr<sub>2</sub>H,  $\gamma$ -ZrH,  $\delta$ -ZrH<sub>1.5</sub> and  $\varepsilon$ -ZrH<sub>2</sub> [12, 11]. In addition, dilute solid  
108 solutions were also simulated in which one hydrogen atom was placed in  $2 \times 2 \times 2$ ,  $3 \times 3 \times 2$  and  $4 \times 4 \times 3$   
109 supercells of  $\alpha$ -Zr, giving concentrations of 5.8 at%H, 2.7 at%H and 1.0 at%H respectively. A further  
110 calculation was carried out in which one atom of H was placed in a  $2 \times 2 \times 2$  supercell of FCC Zr. All of the  
111 solid solution calculations described so far were carried out with H occupancy being investigated on both  
112 octahedral and tetrahedral sites.

113 A different method was used to simulate more disordered structures. As a starting point for the generation  
114 of off-stoichiometric hydride phases, a  $\delta$  hydride structure is built, formed from a  $2 \times 2 \times 2$  supercell of the  
115 primitive cell, with all tetrahedral H sites occupied (giving a formula of ZrH<sub>2</sub>). This is similar to the  $\varepsilon$   
116 hydride, except that the  $c/a$  ratio is 1. A new cell is generated from this input, by giving each H atom a  
117 random chance to be removed of 0.166 (or  $1 - \frac{1.6}{2}$ ). This is repeated to generate a large number of cells, with  
118 the only constraint being that new cells must be unique from previously generated cells. These cells then  
119 undergo geometry optimisation to provide energies for each configuration. No constraints are placed upon  
120 the number of H atoms in any given cell, meaning some cells will have more H than the 1.66 ratio, and some  
121 will have less. Providing the number of cells is large enough, the formulae of the different cells will follow  
122 a normal distribution with a mean of 1.66. A similar method was used with a  $2 \times 2 \times 2$  supercell of  $\alpha$ -Zr,  
123 and a removal probability of 0.89 with single H atom cells discounted. This provides a selection of solid  
124 solution cells where the H exists in small clusters, modally containing 2 H atoms, which are used to bridge  
125 the stoichiometry gap between a dilute solid solution and the  $\zeta$  phase. These sets will have a number of  
126 different possible configurations, which allows examination of how configurationally sensitive the properties  
127 of the hydrides and solid solutions are. Taken together, an arbitrarily large set of these cells provide a more  
128 complete description of the  $\delta$  hydride and a concentrated solid solution than any single periodic calculation.  
129 The advantages of random structure generation have been discussed previously [37].

130 In order to qualify this method against established techniques, the random  $\delta$  hydride set is compared  
131 with SQS generated cells. The SQS technique, as detailed in reference [25], works on the assumption that  
132 in any random arrangement of atoms on a pre-defined set of atomic sites, some clusters of atoms will be  
133 more common than others. The more common clusters are defined by the structure and stoichiometry of  
134 the simulated crystal. Thus, a number of “special” cells can be constructed that comprise the more common  
135 configurations, and less common configurations can be discounted. In this study, 3 different SQS cells are

136 simulated containing 48, 52 and 56 H atoms, along with 32 Zr atoms. The SQS method has been recently  
137 applied to this system in order to model bulk parameters [26]. The 3 most representative SQS cells in that  
138 paper are used again here.

139 Some phases, however, exhibit more order than the  $\delta$  phase, such as the  $\gamma$  and  $\zeta$  phases. Generally, these  
140 phases are simulated as ordered phases with a defined structure and no disorder. However, any real hydride  
141 will likely exhibit a degree of disorder, particularly when a disordered phase can transform to an ordered  
142 phase and vice versa [17]. Thus, a method has been devised to introduce disorder into these structures,  
143 whilst biasing the results towards the known structures. In this “skew-random” method, the starting point  
144 is a cell of the ordered structure. For each occupied H site, a small removal probability of the H atom is  
145 introduced. Likewise, for each unoccupied site, a small chance is created to have a H atom inserted. In  
146 both of these cases the probability of 0.05 was used, as it created a reasonable spread of random structures,  
147 whilst remaining close to the crystallographic form of the hydride. As before, a large number of these cells  
148 were generated and only unique cells are simulated to ensure that the full ensemble of simulations is relevant  
149 to a (partially) disordered hydride. A smaller number of random cells was also generated with no structure  
150 biasing and a probability for removal of 0.5. These were used purely as a comparison with the skew-random  
151 cells.

152 Ultimately, all possible arrangements of H on interstitial sites in Zr exist as points in the configuration  
153 space. Each of the methods described above develops a different sampling of that configuration space, aiming  
154 to ensure that a valid distribution is identified.

### 155 3. Results

#### 156 3.1. Elements and Ordered Crystals

157 In order to ensure the validity of the simulations performed, the physical and chemical properties of the  
158 pure elements in their reference state are presented in Table 1 together with established literature values.  
159 Excellent agreement is achieved on all counts, to within a maximum discrepancy of 1.65%.

160 The enthalpies of formation of different ordered crystals are given in Table 2, following equation:

$$\Delta H_f = \frac{1}{x+y} \left[ E(\text{Zr}_x\text{H}_y) - \left( E(x\text{Zr}) + y\frac{1}{2}E(\text{H}_2) \right) \right] \quad (3)$$

161 where  $E(\text{Zr}_x\text{H}_y)$  represents the energy of the hydride (or solid solution containing H) and the other terms  
162 refer to the pure elements. As the number of atoms in each simulation differs, the formation energy must  
163 be normalised with respect to the number of atoms, in order to not bias the formation energies towards the  
164 larger cells. Solution enthalpies of H atoms in a HCP and an FCC matrix are also presented. Although the  
165 latter configuration is un-physical (pure FCC Zr is not a stable phase, nor observed in real alloys) it does  
166 provide useful comparison points. Although this phase assumes the absorption of H into an FCC lattice,

167 the reference state is still taken to be HCP Zr. This is done to ensure fair comparison with other results  
168 and is based on the assumption that any starting point that could lead to this configuration would still  
169 be based on HCP Zr. As formation energies for FCC solutions must also contain the energy associated  
170 with a HCP  $\rightarrow$  FCC phase change, it is reasonable that the formation energies for the FCC solutions are  
171 higher than their HCP counterparts. The dilute tetrahedral solid solution is of particular importance as it  
172 represents a reference point for comparison in further calculations. The number reported here of  $-0.60$  eV  
173 compares favourably with  $-0.52$  eV from [38],  $-0.604$  eV from [12] and  $-0.464$  eV from [39]. The tetrahedral  
174 site for H occupancy remains the most favourable, in agreement with most prior work [38, 18, 12, 39]. For  
175 the remainder of this work, when considering sites for H occupancy, only the tetrahedral site is considered.  
176 More exotic configurations such as  $H_2$  dimers on interstitial sites have also previously been found to be  
177 unfavourable [12].

178 With regards to the approximate  $\delta$  phase,  $ZrH_{1.5}$ , a conventional unit cell of FCC Zr offers 8 sites for H  
179 occupancy, 6 of which must be filled with the other two vacant. If the system is cubic, then symmetry reduces  
180 the number of configurations to three different arrangements. These arrangements are where the vacancies  
181 are both in the [100], [110] and [111] directions. These are referred to in Table 2 by these directions. The  
182 configuration with the lowest enthalpy of formation is the one in the [111] orientation, where the vacancies are  
183 separated by the longest distance. The energy difference between these states is relatively small, and similar  
184 (but slightly larger) than the average of the energy calculated from using the three SQS configurations.

### 185 *3.2. Statistical Analysis*

186 In order to ensure that the simulations are representative of the disordered system it is important that  
187 a large enough sample of the configuration space is achieved. With this in mind, the statistical parameters  
188 generated in the sets used are shown in Table 3. The  $\delta$  and solid solution series rely on a random distribution  
189 about the selected stoichiometry, while the  $\zeta$  and  $\gamma$  phases use the skew-random method. A large enough  
190 sample has been made when the data set forms a normal distribution centred on the target stoichiometry.  
191 A simple convention for determining normality is a plot of the cumulative distribution probabilities of the  
192 data against theoretical cumulative distribution probabilities generated by a standard normal distribution  
193 [40], with the parameters in Table 3. A straight line fit would represent perfectly normal data. Normality  
194 tests were performed on sets of increasing sample size until a high degree of confidence in normality was  
195 achieved. Figs. 2(a) and 2(b) show normality tests for each set of data, generated from both the stoichiometry  
196 distribution and the formation enthalpy distribution. In both cases, we see all series display a good linear  
197 fit. We report that for sample sizes of 50 cells per set, all datasets showed high coefficients of linear  
198 regression with the lowest  $R^2$  being 0.9602. The average stoichiometry for each set is extremely close to  
199 the experimental formula value considered representative for that hydride structure. This gives confidence  
200 to the hypothesis that this set of randomly generated structures approximates a disordered material when

201 taken as a whole.

### 202 3.3. Enthalpies

203 Relative thermodynamic phase stability can be determined by plotting the formation energy across the  
204 range of compositions, in the form of a convex hull diagram, see Fig. 3. Specifically, this represents a latent  
205 formation enthalpy, as opposed to a free energy. Here, a convex hull is defined as the smallest convex path  
206 to contain all of the available data points, when viewed from below the plot. It is useful, because any  
207 mixture with an enthalpy less negative than the convex hull would be more stable as a mixture of the two  
208 configurations which bound that segment of the hull.

209 In Fig. 3, all enthalpies are negative indicating that there is a general thermodynamic driving force for  
210 formation, which becomes stronger with greater H-content phases. However, the majority of configurations  
211 lie above the convex hull, indicating they are less stable than a mixture of other phases. The configurations  
212 which lie on the convex hull are the 1 at%H solid solution, the stoichiometric and ordered  $\gamma$  hydride, and  
213 the  $\varepsilon$  phase with a  $c/a$  ratio of less than 1. The enthalpies in the stoichiometry range  $\text{ZrH}_{0.01}$  to  $\text{ZrH}_{0.6}$   
214 agree with a similar plot produced by Hollinger *et al.* [41] in terms of the range of formation enthalpies of  
215 the different structures. However, whereas that work noted stable structures in this range, none are found  
216 in the present work. This is almost certainly due to the fact that the work of Hollinger *et al.* was focused  
217 on hexagonal phases, whereas the present work shows that cubic phases out-compete hexagonal structures  
218 in terms of stability. Domain *et al.* [12], provide a similar plot with no convex hull, however adding one  
219 demonstrates the same phases ( $\varepsilon$  and  $\gamma$ ) as stable and by similar energies. This result has also been found  
220 by Zhong and MacDonald [24], who used this data to suggest that the  $\gamma$  phase is thermodynamically stable  
221 below  $\approx 523$  K. This contrasts greatly with Zhu *et al.* [13], who claimed that the  $\delta$  hydride is by far the  
222 most stable hydride, by nearly 8 eV more than the other phases. It is, however, difficult to understand that  
223 result, since the “convex hull” presented was not actually convex, and the magnitude of this number is out  
224 of line with other results [12, 24, 38, 41].

225 Ultimately, hydrides are formed by the precipitation of H from solid solution in the  $\alpha$ -Zr matrix. This  
226 reaction is given by the expression:

$$\Delta E^P = [E(\text{Zr}_x\text{H}_y) + (y)E(\text{Zr}_R)] - [yE(\text{Zr}_R\text{H}) + xE(\text{Zr})] \quad (4)$$

227 Eq. 4 forms the basis of calculating the change in different thermodynamic parameters such as the latent  
228 enthalpy of precipitation. The term  $R$  is the number of Zr atoms in the solid solution reference cell.  
229 Precipitation enthalpies have been calculated using reference solutions containing 96, 36 or 16 atoms of  
230 Zr to one atom of H. This equation is balanced with free Zr on both sides because it ensures that the  
231 reaction maintains reversibility in situations where the concentration is different. As with the formation  
232 enthalpies, these precipitation enthalpies must be normalised to ensure that larger simulations are not shown



233 as having larger enthalpies purely based on their size, and not on changes in composition and thermodynamic  
234 behaviour. To this end, all simulations are divided by the total number of H atoms present in the hydride  
235 phase, and then converted into  $\text{kJ mol}^{-1}$ . Thus, the enthalpies presented hence forth are in units of  $\text{kJ}$   
236  $\text{molH}^{-1}$ , representing the enthalpy change required for one mole of H atoms to precipitate from a solid  
237 solution.

238 The latent enthalpies of precipitation are presented in Fig. 4. As with the formation enthalpies, there is  
239 a general trend that the precipitation of H-rich hydrides is more preferable than H-poor hydrides. On the H  
240 poor side of the graph, solid solutions have more negative enthalpies when they are less concentrated than  
241 the reference solid solution for that series, suggesting a trend towards dilution of H atoms. Moving across  
242 towards products with a greater H content, there is then a peak of unfavourable H clusters around  $\text{ZrH}_{0.2}$ ,  
243 followed by a steady return to the more preferable hydride phases. In particular, the  $\gamma$  phase exhibits the  
244 strongest preference for precipitation, with the most favourable configuration being the structure typically  
245 modelled in other simulation studies, shown in Fig. 1. There is a notable discontinuity in all series at  
246  $\approx \text{ZrH}_{0.75}$ , corresponding to the point where the series switched from modelling HCP hydrides to FCC  
247 hydrides.

248 There are no negative latent enthalpies of precipitation for the precipitations from 1 at%H and 2.7 at%H  
249 solid solutions. However there are for the 5.9 at%H solid solution. It is sensible that increasing the H  
250 content in the Zr lattice increases the impetus for the rearrangement of the H atoms into a hydride, as is  
251 evidenced by the existence of a terminal solubility limit for H in Zr [2]. Overall, this plot is consistent with  
252 H having a bimodal distribution in Zr, preferring to exist either as a sparsely distributed solid solution, or  
253 as a concentrated hydride. A middle-ground between these two modes is unfavourable.

254 So far, this only describes the latent enthalpy with no regards for the effects of temperature. The sensible  
255 enthalpy of precipitation is related to the heat capacities of the products and reactants of the precipitation  
256 reaction. Heat capacities calculated at 298 K are  $23.00 \text{ kJ mol}^{-1} \text{ K}^{-1}$  for  $\alpha\text{-Zr}$  and  $28.64 \text{ kJ mol}^{-1} \text{ K}^{-1}$  for  
257  $\varepsilon \text{ ZrH}_2$  (compared with the available experimental values of  $25.45 \text{ kJ mol}^{-1} \text{ K}^{-1}$  and  $31.08 \text{ kJ mol}^{-1} \text{ K}^{-1}$   
258 [42]). Fig. 5 gives the absolute sensible enthalpies for reference simulations, as they vary with temperature.  
259 The values for the three  $\delta$  phase stoichiometries are calculated using the SQS generated cells. There is a  
260 general trend for increasing sensible enthalpy with increasing H content. The  $\zeta$  phase has a substantially  
261 lower sensible enthalpy than the other hydride phases. As the temperature increases, the variance in sensible  
262 enthalpies decreases. The enthalpy calculated at 0 K represents the zero point energy contribution to the  
263 enthalpy of this system.

264 The absolute sensible enthalpy is of less interest than the change in sensible enthalpy which may drive  
265 precipitation. Using Fig. 5, a surface is generated to describe the relationship between composition, temper-  
266 ature and sensible enthalpy. Using this surface, values are interpolated for sensible enthalpies for all the cells  
267 examined in this work. The enthalpy data is sufficiently close that a simple linear interpolation does not

268 introduce unreasonable variance. Feeding this interpolation into Eq. 4, the sensible enthalpy change during  
 269 precipitation for a variety of different structures and temperatures is generated and plotted in Fig. 6. This  
 270 information is presented only for the precipitation from the 16 atom solid solution. Given that the sensible  
 271 enthalpy is added to the latent enthalpy, in Eq. 1, a negative value of sensible enthalpy represents a driving  
 272 force for precipitation, while a positive value represents a driving force for solution. The sensible enthalpy  
 273 appears to drive the system towards precipitation for all product stoichiometries greater than  $\sim \text{ZrH}_{0.08}$ .  
 274 As temperature increases, the driving force for precipitation also increases. There is a relative increase in  
 275 this driving force for stoichiometries of  $\sim \text{ZrH}_{0.4}$ , which corresponds roughly with the stoichiometries found  
 276 in the  $\zeta$  phase hydrides. The sensible enthalpy then becomes less negative for stoichiometries appropriate  
 277 to  $\gamma$  hydrides before reducing slightly for hydrides with even greater H content.

### 278 3.4. Entropy

279 As described previously, computing the free energy of a reaction requires a description of the entropy as  
 280 well as the enthalpy. In this study, we examine two sources of entropy - the vibrational and the configura-  
 281 tional.

282 Configurational entropy stems from the disorder available when the structure may have multiple different  
 283 forms. It is quantified by the Boltzmann entropy equation:

$$S_c = k \ln \Omega \quad (5)$$

284 where  $\Omega$  is defined as the number of different configurations or micro-states in which the system may  
 285 be arranged and  $k$  is Boltzmann's constant. In an atomistic context, the number of different structure  
 286 configurations is given by adopting the standard permutations expression:

$$\Omega = \frac{(N_V + N_H)!}{N_V! N_H!} \quad (6)$$

287 where  $N_V$  is the number of potential H sites which are vacant, while  $N_H$  is the number of H atoms.

288 As before, the primary concern is not the absolute entropy, but the change in entropy during precipitation.  
 289 Using the entropy calculated in Eq. 5 into the precipitation Eq. 4 (with the H coming from the 16 atom Zr  
 290 cell), the change in configurational entropy is determined across a range of stoichiometries, and displayed  
 291 in Fig. 7. These entropies are presented as a  $T\Delta S$  product. As entropies are subtracted from enthalpies  
 292 to generate a free energy, a negative value indicates a driving force towards solution while a positive value  
 293 drives towards precipitation. For non-zero temperatures, we see that the configurational entropy represents  
 294 a driving force for solution, that, of course, increases with increasing temperature. There is a notable  
 295 discontinuity when the simulated series shift to modelling FCC hydrides. This is because the FCC structure  
 296 has more tetrahedral sites per Zr atom, which are considered as possible sites for H occupancy (i.e. it

297 offers greater configurational options). Thus, the shift from HCP to FCC is favoured by the configurational  
298 entropy and this driving force increases with temperature.

299 The final contribution examined in this work is the vibrational entropy. Vibrational entropies are shown  
300 in Fig. 8 for the same reference cells as used in calculating the sensible enthalpy. Vibrational entropies  
301 at 298 K are  $37.52 \text{ J mol}^{-1} \text{ K}^{-1}$  for  $\alpha$ -Zr and  $31.387 \text{ J mol}^{-1} \text{ K}^{-1}$  for  $\epsilon$  ZrH<sub>2</sub>, compared with the available  
302 experimental values of  $39.144 \text{ J mol}^{-1} \text{ K}^{-1}$  and  $35.154 \text{ J mol}^{-1} \text{ K}^{-1}$  respectively [42]. It should be noted  
303 that experimental results will include other forms of entropy (such as that generated by intrinsic defects  
304 on the Zr lattice), hence it is reasonable that the theoretical results are slightly smaller than experimental  
305 values. Fig. 8 demonstrates a decreasing vibrational entropy with increasing H content. Similar to the  
306 calculation of sensible enthalpies, this plot is used to interpolate values from a temperature-composition-  
307 entropy surface. Applied across the range of compositions, the vibrational entropy is given in Fig. 9 as a  
308  $T\Delta S$  product. This plot shows negative values for all compositions above  $\sim \text{ZrH}_{0.08}$ , and temperatures  
309 above 0 K. This is consistent with the vibrational entropy driving the reaction towards solution, with the  
310 effect becoming stronger with increasing temperature. The vibrational entropy change during precipitation  
311 is positive for dilute solid solutions, becomes negative for non-dilute solutions, and becomes more negative  
312 as H content increases. There is a decrease in the magnitude of the entropy change for hydrides of around  
313  $\sim \text{ZrH}_{1.5}$ , suggesting vibrational entropy may contribute to stabilising the  $\delta$  phase.

### 314 3.5. Free Energy

315 With the change in both the enthalpy and entropy terms calculated for the precipitation reaction, the  
316 overall free energy change can be calculated from Eq. 2. It is sometimes stated that vibrational entropies and  
317 sensible enthalpies are too small to be important in this system and other hexagonal metals [43]. Although  
318 this may be true for predicting if hydrides occur at all, and for determining energies when one reactant is  
319 in a different state (eg. H<sub>2</sub> gas), in a system with multiple solid phases, containing subtle interactions, the  
320 magnitude of these other terms may be important. Given that the sensible enthalpy and configurational  
321 and vibrational entropy terms (as  $T\Delta S$  products) are all within the range of  $-20$  to  $40 \text{ kJ molH}^{-1}$ , none of  
322 these variables can be discounted and all have a part to play in determining phase stability.

323 In Figs. 10(a)–10(c), the lowest energy configuration from each data set is plotted as a free energy, with  
324 respect to the stoichiometry. Fig. 10(a) represents the free energy of precipitation from the 96 atom cell,  
325 Fig. 10(b), is from the 36, and Fig. 10(c) is from the 16. In the first of these plots, Fig. 10(a), the free energy  
326 remains positive across the entire stoichiometry range. Temperature raises the energy by over three times  
327 the 0 K values. As with all these plots, there appear to be five distinct regions, defined by stoichiometry.  
328 The first occurs between  $\text{ZrH}_0 \rightarrow \text{ZrH}_{0.1}$ . Here, increasing the stoichiometry drastically increases the free  
329 energy of precipitation, suggesting that concentrating the H in the lattice is energetically unfavourable.  
330 This reaches a relatively flat region 2, made up of clusters of H atoms. This is particularly unfavourable,

331 suggesting that H prefers to remain distributed. There is then a significant drop in free energy entering into  
332 region 3. The start of region 3 contains both H clusters, and sub-stoichiometric  $\zeta$  hydrides as modelled by  
333 the skew-random technique. The  $\zeta$  hydrides are more energetically favourable, and have a minimum energy  
334 point at  $\text{ZrH}_{0.5}$ , for the expected structure of the  $\zeta$  hydrides. However, as H content continues to increase,  
335 the free energy rises again and is out-competed by the sub-stoichiometric  $\gamma$  phase at the start of region  
336 4. This phase remains competitive until region 5 is entered, where stoichiometries are closer to that of the  
337  $\delta$  phase than  $\gamma$ . Beyond this, energies remain relatively flat until the terminating  $\varepsilon$  phase is reached. As  
338 temperatures increase, region 5 begins to show a slight upwards slope, signifying it is more preferable to  
339 precipitate larger quantities of H-poor hydrides, than smaller quantities of H-rich hydrides.

340 Assuming an initial concentration of 2.7 at%H, see Fig. 10(b), the results are similar to those for 1.0 at%H,  
341 however precipitation energies for the  $\gamma$  and  $\varepsilon$  phases are now just about zero or marginally negative at 0 K.  
342 At higher temperatures, precipitation of all the hydrides remains unfavourable, and the reaction is still  
343 driven towards solid solution. The free energies are lower overall, and the difference brought about by  
344 increasing temperature is smaller.

345 Finally, the free energies drop significantly when moving to an initial concentration of 5.9 at %H.  
346 Fig. 10(c), shows negative precipitation energies across the full range of stoichiometry and temperatures,  
347 with the exception of stoichiometries in the range of  $\text{ZrH}_{0.1}$  to  $\text{ZrH}_{0.4}$  (region 2). Below this, there is still a  
348 thermodynamic driving force for keeping H dispersed, but above this, there is impetus for hydride forma-  
349 tion. As in all prior plots, increasing temperature cause free energies to become more positive and drives  
350 solution. At the higher temperatures, the energy of the  $\zeta$  phase increases to the point where its precipi-  
351 tation is no longer thermodynamically favourable. The tendency for regions 4 and 5 to slope upwards at  
352 higher temperatures is even greater when precipitation occurs from a more concentrated initial solution.  
353 The most favourable phases are  $\gamma$  and  $\varepsilon$ , although higher temperatures seem to favour  $\gamma$  hydrides. Overall,  
354 this remains consistent with a bimodal H distribution, as described previously.

## 355 4. Discussion

### 356 4.1. Hydrogen in zirconium

357 It is well established that there is a strong thermodynamic impetus for H to become sequestered in a Zr  
358 lattice. This is corroborated by the energy values given for H solution in Table 2, which are all substantially  
359 negative. If we compare this for any of the values for precipitation, we see that the impetus of adding H to  
360 the Zr lattice is substantially greater than the energy of rearranging or precipitating the H once it is already  
361 in the lattice. This means that if the thermodynamic values for  $\text{H}_2$  gas are less affected by temperature  
362 than the solid solution values are, it would be expected that H will continue to be added to Zr over the life  
363 of the cladding, steadily driving up concentration.

364 In Figs. 10(a) and 10(b), the lowest free-energy configuration is the 1.0 at%H solid solution, suggesting  
365 that H will preferentially form a dilute solid solution if possible. Temperature effects drive this behaviour  
366 further, in that the energy of the 1.0 at%H solid solution becomes more negative and the more H rich solid  
367 solutions become more positive. In order to produce this behaviour, there must be some sort of interaction  
368 between H atoms that raises the energy of the system. Given that electron interactions have been previously  
369 demonstrated to be extremely localised to H atoms in the H-Zr system [12], it is unlikely that the chemistry  
370 of H is driving this response. This leaves geometrical factors and most notably stress. It is possible that  
371 the stress fields created by the insertion of H atoms into nearby interstitial positions in the Zr lattice are  
372 mutually repulsive.

#### 373 4.2. Implications for hydride precipitation

374 If there is an initial impetus for H atoms to remain in solid solution, then given that hydrides have  
375 been noted to form experimentally, at some point conditions *must* change to favour hydride formation. As  
376 more and more H atoms are absorbed by the Zr, the barrier for H atoms to congregate must be overcome.  
377 In Fig. 10(c), a high starting concentration of 5.9 at%H provides this condition. This suggests at some  
378 point between 307 ppm and 690 ppm, that H atoms will be so numerous that they will be pushed past their  
379 mutually repulsive behaviour and will start to form hydrides. These values are significantly higher than those  
380 measured globally in actual alloys, implying Zr has a much higher local H carrying capacity than suggested  
381 experimentally [44]. If this is the case, in order for precipitation to occur, forces beyond those predicted in  
382 these DFT simulations must generate a driving force for concentration, and hence precipitation. Given this  
383 case, it is possible that larger scale stress states, such as those provided by defects or cracks, could lessen  
384 this mutually repulsive force, allowing H atoms to diffuse together more easily. The idea that stress impacts  
385 diffusion is not new, and has been suggested as a key part of the mechanism behind DHC [1, 44, 45]. It is  
386 reasonable that the Zr lattice around an interstitial H atom is in a state of compression. Given this, a tensile  
387 stress field would provide a nullifying effect on the repulsive interaction. Coupled with areas that are not  
388 under stress, there would be an impetus for H atoms to move away from regions where H atoms are in close  
389 proximity and not under tension, towards areas where they can congregate more favourably. This argument  
390 is based upon the existence of the aforementioned barrier to association, and provides an area which can be  
391 investigated in future studies.

392 Temperature also has the effect of driving the system towards solution, by raising the composition  
393 of the first point where hydriding may occur. In the room temperature series (300 K), the first hydride  
394 with a negative free energy of precipitation has a composition of about  $\text{ZrH}_{0.43}$ , while in the operating  
395 temperature series, this is raised to over  $\text{ZrH}_{0.7}$ . The main reason for this increase is entropic, in that both  
396 the configurational and vibrational entropy drive the reaction towards solution.

### 397 4.3. Zirconium Hydrides

398 The free energy curves produced in this study can be used to predict which hydride phase will precipitate,  
399 should precipitation occur. At 0 K, The  $\gamma$ ,  $\delta$  and  $\varepsilon$  hydrides present similar formation energies, suggesting  
400 that thermodynamically they may coexist at equilibrium, as observed experimentally [4, 46, 47], if other  
401 factors such as local stress and interfacial energy are disregarded. On the other hand, the  $\zeta$  phase presents  
402 significantly less favourable formation energy compared to the other hydrides, yet a local minima is found  
403 in the free energy curve about the  $\text{ZrH}_{0.5}$  composition, suggesting that the  $\zeta$  hydride may be metastable, in  
404 agreement with previous work [11]. Fig. 10(c) indicates that as temperature increases, the stability of the  $\gamma$   
405 phase relative to  $\varepsilon$  increases. The primary driver of this is the configurational entropy. Thus, in reactor, we  
406 would expect to see  $\gamma$  phase hydrides, while at room temperature or lower, hydrides with a greater H content  
407 are favoured. This is in accord with the experimental observation that  $\gamma$  phase hydrides have been observed  
408 to form primarily in rapidly cooled samples [16, 48, 49], but samples with a relatively low H content allowed  
409 the formation of  $\gamma$  hydrides under slower cooled conditions [6, 10, 14]. There are, however, other factors in  
410 the precipitation of hydrides that are difficult to investigate using DFT, such as stress states caused by the  
411 anisotropic expansion of  $\alpha$ -Zr grains and by the nucleation and growth of the hydrides themselves [4, 17], the  
412 formation of Zr/hydride interfaces [46] and the effect of matrix hardening [14, 50, 51, 52]. Given the small  
413 differences in free energy between the  $\gamma$ ,  $\delta$  and  $\varepsilon$  hydride phases reported in the current work, it is expected  
414 that these factors may play an important role in the thermodynamics of hydride precipitation, dictating  
415 which phase is favoured over others [16, 49] or whether they may coexist in the same sample [4, 15, 34].

## 416 5. Conclusion

417 This work has used DFT to investigate the thermodynamics of the precipitation of Zr hydrides over  
418 a range of temperatures, compositions and starting solid solution concentrations. The use of statistically  
419 significant numbers of randomly generated configurations has been coupled with SQS cells to ensure that  
420 disordered cells are modelled accurately. This investigation has led to the following conclusions:

- 421 • H favours a bimodal distribution within the Zr lattice. At low concentration, it prefers to maintain  
422 a dilute, non-clustered configuration, with a high energy barrier to hydride formation. As more H is  
423 absorbed by the Zr this barrier is overcome and hydride precipitation become energetically favourable.
- 424 • The predicted concentration of the H solutions required to initiate precipitation is greater than ob-  
425 served experimentally, suggesting there may be additional mechanisms needed to enhance local H  
426 concentration to drive precipitation. Stress may play a part in this.
- 427 • The calculation of latent enthalpies alone are insufficient to fully describe this system. Vibrational  
428 entropy, configurational entropy and sensible enthalpy are important for dealing with phase stabilities

429 of precipitates and solid solutions.

- 430 • Sensible enthalpies drive the reaction towards precipitation and are particularly significant for the  $\zeta$   
431 hydride.
- 432 • Configurational entropy drives the system towards solution. They are particularly significant when  
433 contemplating the difference between HCP and FCC based hydrides.
- 434 • Vibrational entropy and thus temperature drives the system towards solution.
- 435 • Generally, the  $\gamma$  phase is the most stable, suggesting other mechanisms, (such as precipitate interface  
436 lattice strain) may be responsible for the observed presence of  $\delta$  hydrides.

### 437 **Acknowledgements**

438 Special thanks go to M. J. D. Rushton for his generous assistance. S. C. Lumley and M. R. Wenman  
439 acknowledge financial support from the MoD from a UDS grant. M. R. Wenman acknowledges support from  
440 EDF Energy through an industrial Fellowship award. S. T. Murphy and P. A. Burr acknowledge financial  
441 support through an EPSRC grant (EP/I003320/1) and ANSTO, respectively. All authors acknowledge the  
442 use of Imperial College's high performance computing centre.

- 443 [1] Puls M P 2012 *The effect of hydrogen and hydrides on the integrity of zirconium alloy components: delayed hydride*  
444 *cracking* (Springer)
- 445 [2] Kearns J J 1967 At. Energ. **22** 292-303
- 446 [3] Kearns J J 1972 J. Nucl. Mater. **43** 330-338.
- 447 [4] Barrow A T W, Toffolon-Masclat C, Almer J and Daymond M R 2013 J. Nucl. Mater. **43** 395-401
- 448 [5] Mallett M W and Albrecht W M 1957 J. Electrochem. Soc. **104(3)** 142
- 449 [6] Ells E 1968 J. Nucl. Mater. **28** 129-151
- 450 [7] Raynauld P and Bielen A 2011 *Cladding hydrogen based regulations in the United States: Water Reactor Fuel Performance*  
451 *Meeting* (Chengdu, China)
- 452 [8] Kessler J and Einziger R 2002 *Technical Bases for Extended Dry Storage of Spent Nuclear Fuel*, EPRI (Palo Alto, CA,  
453 USA)
- 454 [9] Okamoto H 2006 J. Phase. Equilib. Diff. **27(5)** 548-549
- 455 [10] Weatherly G C 1981 Acta Metall. **29(3)** 501-512
- 456 [11] Zhao Z, Morniroli J P, Legris A, Ambard A, Khin Y, Legras L and Blat-Yrieix M 2008 J. Microsc. **232(3)** 410-21
- 457 [12] Domain C, Besson R and Legris A 2002 Acta Mater. **50(13)** 3513-3526.
- 458 [13] Zhu W, Wang R, Shu G, Wu P and Xiao H 2010 J. Phys. Chem. C **114(50)** 22361-22368
- 459 [14] Lanzani L and Ruch M 2004 J. Nucl. Mater **324(2-3)** 165-176
- 460 [15] Root J H and Fong R W L 1996 J. Nucl. Mater **232** 75-85
- 461 [16] Nath B, Lorimer G W and Ridley N 1975 J. Nucl. Mater. **58** 153-162
- 462 [17] Steuwer A, Santisteban J, Preuss M, Peel M, Buslaps T and Harada M 2009 Acta Mater. **57(1)** 145-152
- 463 [18] Burr P A, Murphy S T, Lumley S C, Wenman M R and Grimes R W 2013 Corros. Sci. **69** 1-4
- 464 [19] Fukai Y, 1993 *The metal-hydrogen system* (Springer Verlag)
- 465 [20] Glazoff M V 2013 *Modeling of Some physical properties of zirconium alloys for nuclear applications in support of UFD*  
466 *campaign* Technical Report (Idaho National Laboratory)
- 467 [21] Glazoff M V, Tokuhira A, Rashkeev S N and Sabharwall P 2014 J. Nucl. Mater. **444(1-3)** 65-75
- 468 [22] Ackland G 1998 Phys. Rev. Lett. **80(10)** 2233-2236
- 469 [23] Blomqvist J, Olofsson J, Alvarez A and Bjerk C 2012 *Structural and thermodynamical properties of zirconium hydrides*  
470 *from first principles* 15th international Conference on Environmental Degradation of Materials in Nuclear Power Systems-  
471 Water Reactors
- 472 [24] Zhong Y and MacDonald D D 2012 J. Nucl. Mater. **423** 87-92
- 473 [25] Zunger A, Wei S, Ferreira L G and Bernard J E 1990 Phys. Rev. **65(3)** 353-356
- 474 [26] Wang H, Chroneos A, Jiang C and Schwingenschlögl U 2013 Phys. Chem. Chem. Phys. **15(20)** 7599-603
- 475 [27] Mao Z, Seidman D N and Wolverton C 2013 APL Mater. **1** 042103.
- 476 [28] Akbarzadeh A R, Wolverton C and Ozolins V 2009 Phys. Rev. B **79** 184102
- 477 [29] Clark S J, Segall M D, Pickard C J, Hasnip P J, Probert M J, Refson K and Payne M C 2005 Zeitschrift für Kristallographie  
478 **220** 567-570
- 479 [30] Vanderbilt D 1990 Phys. Rev. B **41(11)** 7892-7895
- 480 [31] Monkhorst H and Pack J 1976 Phys. Rev. B **13(12)** 5188-5192
- 481 [32] Methfessel M and Paxton A 1989 Phys. Rev. B **40(6)** 3616-3621
- 482 [33] Pfrommer B G, Cote M, Louie G S and Cohen M L 1997 J. Comput. Phys. **131** 133-140
- 483 [34] Barrow A T W, Korinek A and Daymond M R 2013 J. Nucl. Mater. **432(1-3)** 366-370
- 484 [35] Baroni S, de Gironcoli S and Corso A 2001 Rev. Mod. Phys. **73(2)** 515-562
- 485 [36] Frank W, Elsässer C and Fähnle M 1995 Phys. Rev. Lett. **74(10)** 1791-1794



- 486 [37] Pickard C J and Needs R J 2011 J. Phys. Cond. Mat. **23(5)** 053201
- 487 [38] Udagawa Y, Yamaguchi M, Abe H, Sekimura N and Fuketa T 2010 Acta Mater. **58(11)** 3927-3938
- 488 [39] Burr P A, Murphy S T, Lumley S C, Wenman M R and Grimes R W 2013 J. Nucl. Mater. **443(1)** 502-506
- 489 [40] Chambers J, Cleveland W, Kleiner B and Tukey P 1983 *Graphical methods For data analysis* (Wadsworth)
- 490 [41] Holliger L, Legris A and Besson R 2009 Phys. Rev. B **80(9)** 1-9
- 491 [42] Lide D R 1999 *Handbook of Chemistry and Physics* 80th Ed CRC Press LLC
- 492 [43] K. M. Nicholson, D. S. Sholl, Phys. Rev. B (2012), 86, 134113.
- 493 [44] McRae G A, Coleman C E and Leitch B W 2009 J. Nucl. Mater. **396** 130-143
- 494 [45] Puls M P 2009 J. Nucl. Mater. **393(2)** 350-367
- 495 [46] Barraclough K and Beevers C, 1970 J. Nucl. Mater. **34** 125-134
- 496 [47] Veleva M, Arsene S, Record M, Bechade J L and Bai J 2003 Metall. Mater. Trans. A **34**(March) 567-578
- 497 [48] Bradbrook J, Lorimer G and Ridley N, 1972 J. Nucl. Mater. **42** 142-160
- 498 [49] Northwood D O, 1976 J. Less Common Met. **48(1)** 173-175
- 499 [50] Cann, C D, Puls M P, Sexton E E and Hutchings W G, 1984 J. Nucl. Mater. **126(3)** 197-205
- 500 [51] Perovic V, and Weatherly G, 1992 Acta Metall. Mater. **40(2)** 363-372
- 501 [52] Tulk E, Kerr M and Daymond M R, 2012 J. Nucl. Mater. **425(1-3)** 93-104
- 502 [53] Goldak J, Lloyd L T and Barrett C S 1966 Phys. Rev. **144(2)** 480-484
- 503 [54] Mc Quarrie D A and Simon J D 1997 *Physical chemistry: A molecular approach* 1st ed (University Science Books)

Table 1: Crystallographic and thermodynamic properties of Zr and H. The bracketed value for  $\alpha$  Zr includes the zero point energy component of atomic vibrations.

	Property	Predicted Value	Literature
Zr (HCP)	$a$ (nm)	0.322	0.323 [53]
	$c$ (nm)	0.520	0.5145 [53]
	$E_{\text{vaporisation}}$ (eV/atom)	6.20 (6.24)	6.24 [42]
Zr (FCC)	$a$ (nm)	0.641	—
	$E_f^{\text{FCC}} - E_f^{\text{HCP}}$ (eV/atom)	0.04	—
H (Gas)	Bond Length (pm)	752	746 [42]
	$E_{\text{disassociation}}$ (eV/atom)	4.53	4.52 [42]
	Vibrational Frequency ( $\text{cm}^{-1}$ )	4328.42	4401.21 [54]

Table 2: Enthalpies and lattice parameters of ordered crystals.

Structure	at.% H	$a$ (nm)	$c$ (nm)	$H_{\text{sol}}$ (eV)	$H_f$ (eV/atom)
HCP-Zr(H) (tetrahedral site)	1	0.323	0.517	-0.60	—
HCP-Zr(H) (octahedral site)	1	0.323	0.517	-0.56	—
FCC-Zr(H) (tetrahedral site)	11	0.323	—	-0.19	—
FCC-Zr(H) (octahedral site)	11	0.322	—	-0.43	—
$\zeta$ Hydride	25	0.325	1.078	—	-0.23
$\gamma$ Hydride	50	0.457	0.501	—	-0.44
$\delta$ Hydride [100]	60	0.475	0.483	—	-0.50
$\delta$ Hydride [110]	60	0.469	0.494	—	-0.51
$\delta$ Hydride [111]	60	0.477	—	—	-0.52
$\delta$ Hydride (SQS Average)	60	0.478	—	—	-0.53
$\varepsilon$ Hydride	66	0.500	0.442	—	-0.59

Table 3: Statistical values collected from the different data sets used in this work.  $N$  is the size of the set,  $\sum H$  is the total number of H sites,  $x_{stoich}^{min}$  and  $x_{stoich}^{max}$  are the lower and upper ranges of the stoichiometry,  $\bar{x}_{stoich}$  is the arithmetic mean of the stoichiometry and  $\sigma_{stoich}$  is the standard deviation from the mean.

	$N$	$\sum H$	$x_{stoich}^{min}$	$x_{stoich}^{max}$	$\bar{x}_{stoich}$	$\sigma_{stoich}$
Solid solution	50	800	0.13	0.50	0.19	0.08
$\zeta$ hydride	50	800	0.44	0.88	0.57	0.09
Randomised $\gamma$	15	480	0.63	1.25	1.00	0.16
$\gamma$ hydride	50	1600	0.75	1.38	1.03	0.18
$\delta$ hydride	50	1600	1.25	1.88	1.66	0.16
SQS $\delta$ hydride	3	192	1.50	1.75	1.63	0.10

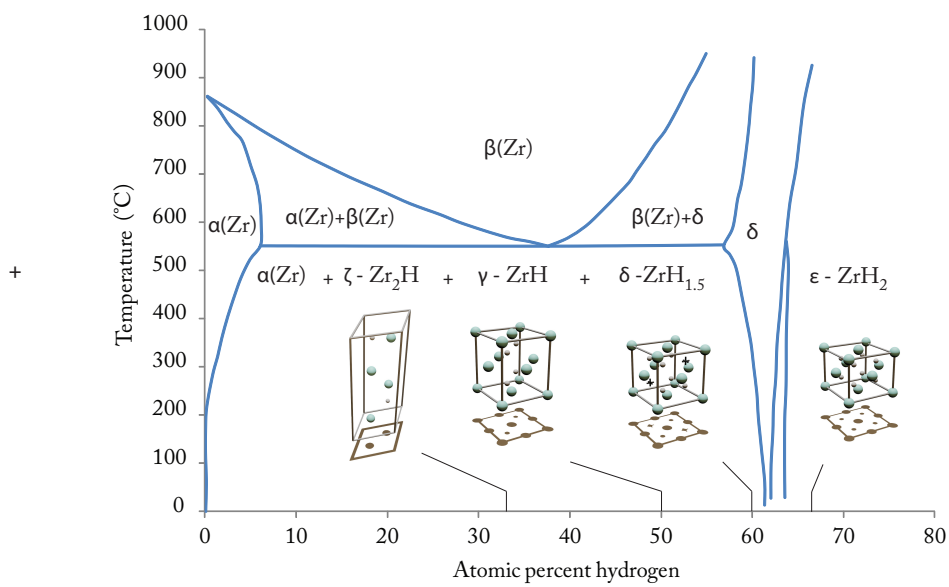
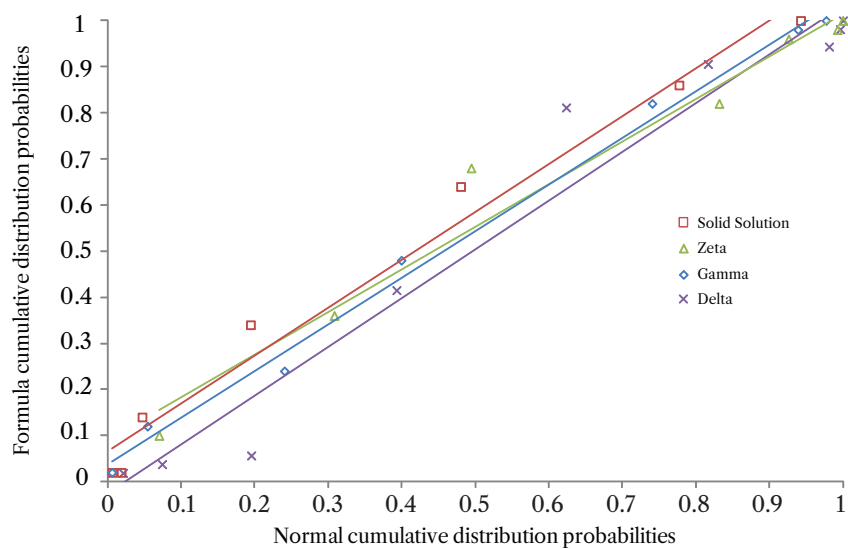
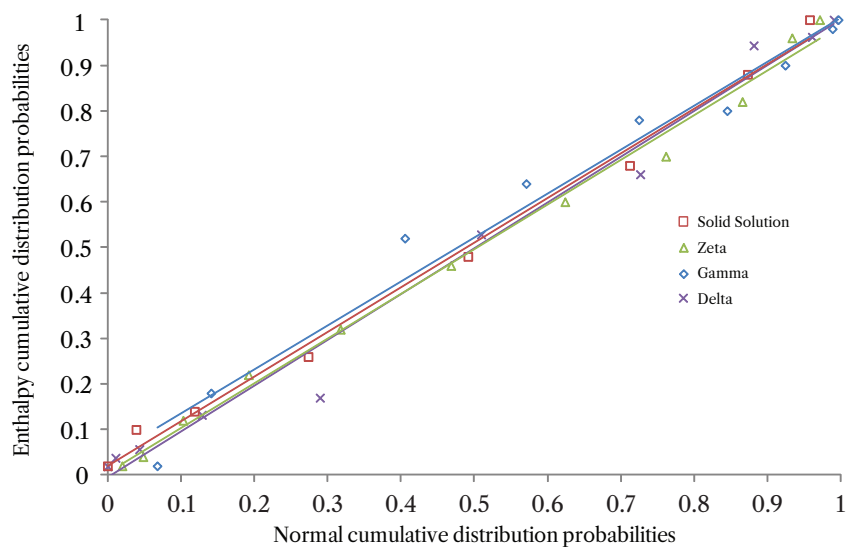


Figure 1: Structures and formulae of different hydrides found in the Zr-H system. The Zr and H atoms are represented by the larger and smaller spheres respectively. The  $\delta$  Hydride shown here is as commonly simulated, while real  $\delta$  phase hydrides have a formula of  $\text{ZrH}_{1.6}$  and have H atoms arranged randomly across all tetrahedral sites, including the black crosses shown in the diagram. The phase diagram has been reproduced from [9].



(a) Frequency distribution analysis of the variation of  $x$  in  $ZrH_x$ .



(b) Frequency distribution analysis of formation enthalpies.

Figure 2: Normality test plots for the structures generated in this study.

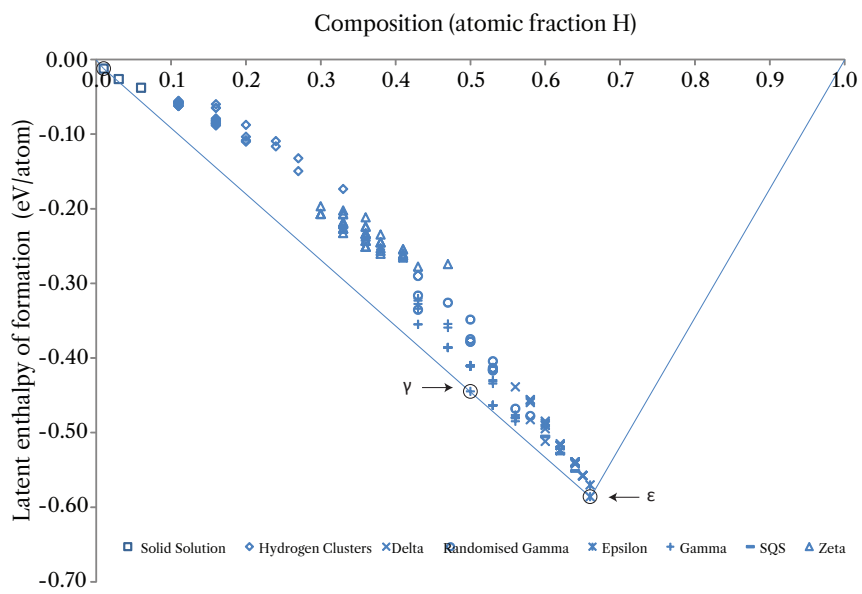


Figure 3: The normalised latent enthalpy of formation from pure elements for all structures studied in this work. The shape of the marker indicates which simulation series it belongs to. Circled points rest on the convex hull.

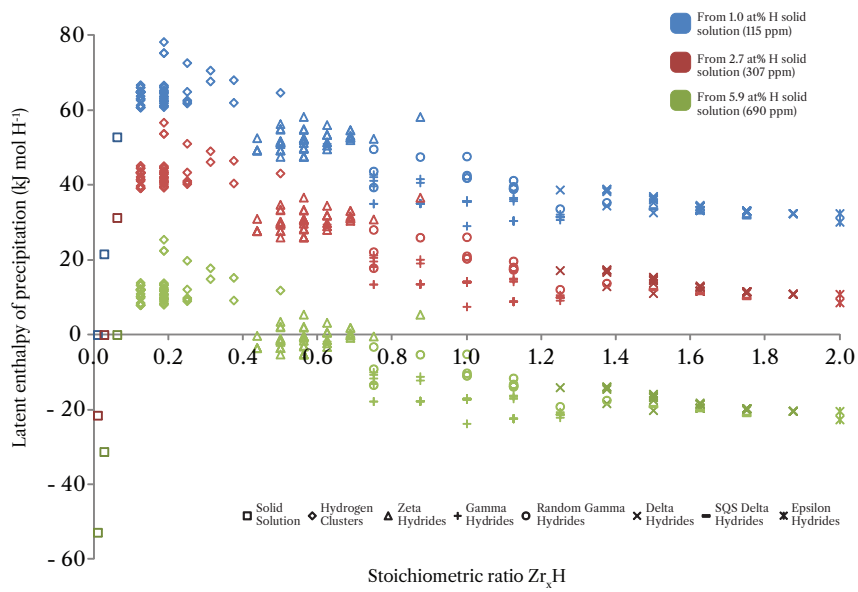


Figure 4: The normalised latent enthalpy for all structures studied in this work. The shape of the marker indicates which simulation series it belongs to, and the colour indicates the concentration of the initial solid solution. These numbers are normalised with respect to the number H atoms precipitated.

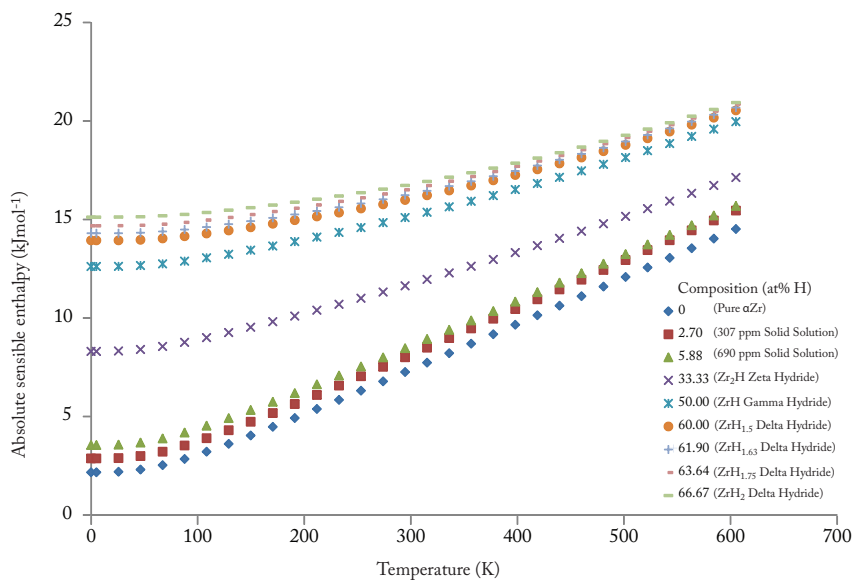


Figure 5: The absolute sensible enthalpy plotted against temperature for a variety of reference simulations. The temperature-composition-enthalpy surface resultant from this data is used to interpolate sensible enthalpies for further calculations.

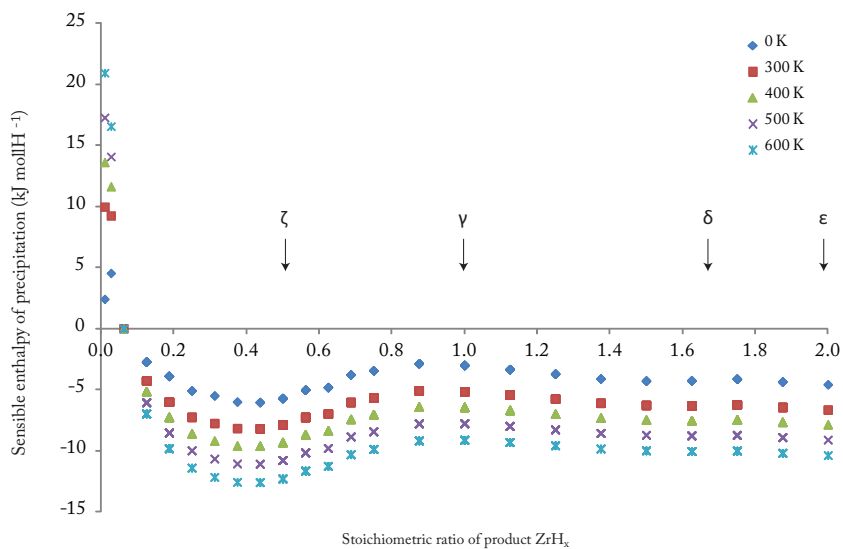


Figure 6: The sensible enthalpy change during precipitation as a function of stoichiometry. These numbers are normalised with respect to the number of H atoms precipitated.



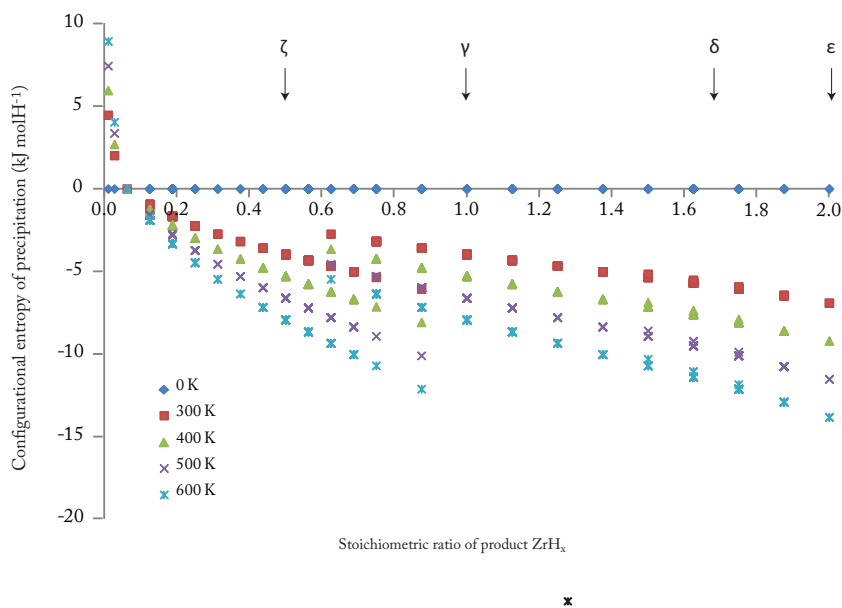


Figure 7: The configurational entropy change during precipitation as a function of stoichiometry. These numbers are normalised with respect to the number of H atoms precipitated. It should be noted that these are presented as a  $T\Delta S$  product.

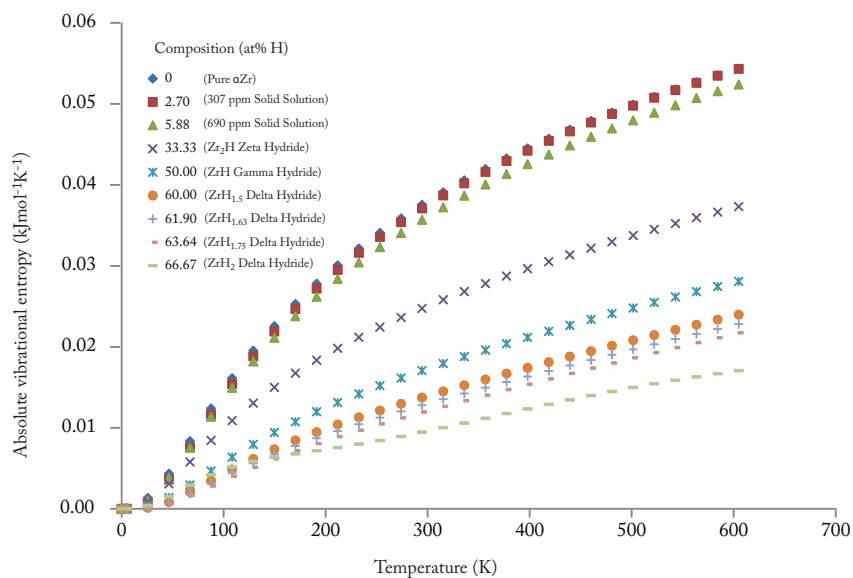


Figure 8: The absolute vibrational entropy plotted against temperature for a variety of reference cells. The temperature-composition-entropy surface resultant from this data is used to interpolate vibrational entropies for further calculations.

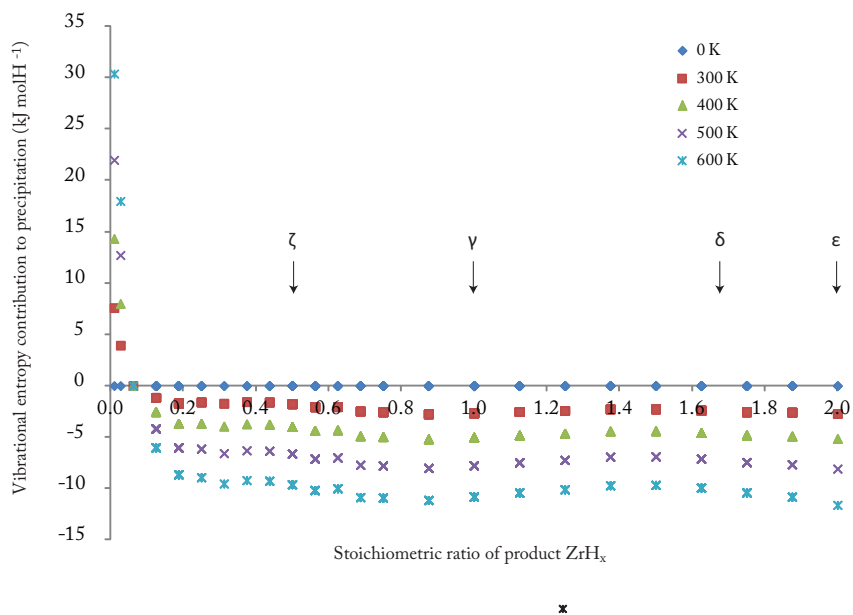
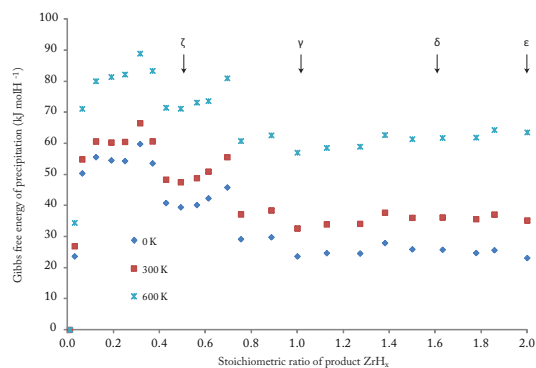
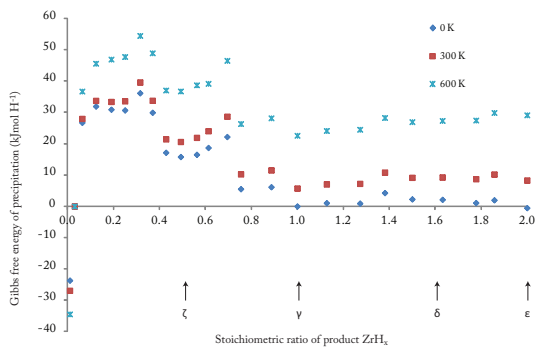


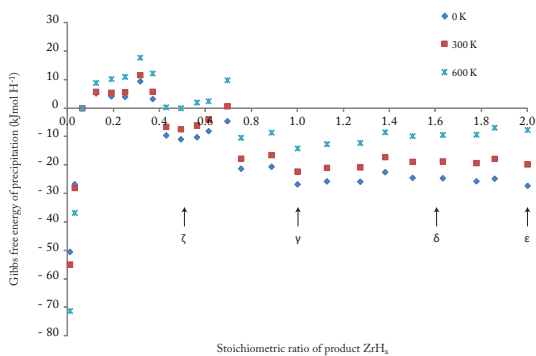
Figure 9: The vibrational entropy change during precipitation as a function of stoichiometry. These numbers are normalised with respect to the number of H atoms precipitated. It should be noted that these are presented as a  $T\Delta S$  product.



(a) Precipitation from a 1.0 at%H solid solution.



(b) Precipitation from a 2.7 at%H solid solution.



(c) Precipitation from a 5.9 at%H solid solution.

Figure 10: The final Gibbs free energy of precipitation, as a function of stoichiometry, from different starting concentrations. These numbers are normalised with respect to the number of H atoms precipitated.